Faraday screen sheaths and impurity production during ion cyclotron heating

1990 Nucl. Fusion 30 845

(http://iopscience.iop.org/0029-5515/30/5/004)

FARADAY SCREEN SHEATHS AND IMPURITY PRODUCTION DURING ION CYCLOTRON HEATING

J.R. MYRA, D.A. D'IPPOLITO
Lodestar Research Corporation,
Boulder, Colorado

M.J. GERVER
Massachusetts Institute of Technology,
Cambridge, Massachusetts

United States of America

ABSTRACT. When a plasma interacts with a material surface subject to an applied voltage, a sheath results. A one-dimensional model, specific to the magnetized ion sheath, is developed and applied to the radiofrequency (RF) sheath which forms near the Faraday screen of an ion cyclotron heating antenna. The RF sheath rectification of the applied voltage is shown to provide a large DC potential drop which can accelerate ions and cause sputtering. Numerical estimates of the high-Z impurity influx are compared with fast wave experiments, and it is concluded that the DC acceleration mechanism is a plausible explanation for the observed high-Z impurity release. Means of controlling the sputtering are examined, including operating with low densities at the Faraday screen.

1. INTRODUCTION

Heating by waves in the ion cyclotron range of frequencies (ICRF) is a promising auxiliary heating method for reactor plasmas because of its economy and the capability of heating deep within the plasma core. A topic of considerable contemporary interest is to understand the impurity generation that is often observed in conjunction with ICRF heating in present day experiments [1–8]. As with other heating methods, high-Z impurities are of particular concern. On reaching the hot core plasma, they can cause degradation by radiating a fraction of the input ICRF power. They also can cause disruptions, contribute to dilution of the deuterium fuel in a fusing plasma and enhance neoclassical transport (both by increasing Z_{eff} and because collisions between *unlike* ion species contribute directly to particle transport).

It is generally believed, and has been shown in specific cases [1, 4], that the Faraday screen of a powered antenna is one source of high-Z impurity atoms. It is this source of radiofrequency (RF) induced impurities that is the subject of the present paper. Although operational techniques such as carbonization and antenna phasing [1, 7] have been successful at reducing the high-Z impurity influx, a detailed understanding of the mechanism of impurity production may allow other, and perhaps preferable, solutions. In this paper, we consider a mechanism based on the RF sheath. The physics of the RF sheath is investigated in detail, and particular emphasis is placed on the dependence of the sheath potential on plasma density. The rich and complex physics of the RF sheath model developed here provides key insights into the JET experimental database on impurity generation by powered ICRF antennas and serves as essential input into a model of the scrape-off layer (SOL) that is being developed [9].

To set the present work in the proper context and to avoid confusion in comparing the present model with the experimental data, one must distinguish between measurements of the metal impurity *generation* at the antenna and measurements of the impurity *concentration* in the plasma core. The present work relates only to the former question, which must be understood before the latter question can be addressed. It must be emphasized that the impurity concentration in the core plasma cannot be simply related to the local generation mechanism at the Faraday screen because of (i) plasma screening of the impurities by ionization and subsequent deposition on the limiters, (ii) resputtering of Faraday screen material from other surfaces (antenna protection tiles or nearby limiters), (iii) core transport which depends on the operational regime of the tokamak.

Several mechanisms which could lead to physical sputtering of impurities from the Faraday screen have already been proposed [10–12]; these are mechanisms

which can produce energetic ion projectiles and hence enhanced sputtering. Typically, ion energies of the order of a few hundred eV are required for substantial sputtering yields [13]. These energies are in excess of those generated by ions falling down the conventional Debye-Bohm sheath (where the potential drop is a few times kT_e) if temperatures in the SOL are in the vicinity of a few tens of eV, as is normally the case in the absence of RF.

Acceleration of impurity ion species which satisfy the conditions for ion cyclotron harmonic resonance has been proposed by Puri [10]. Itoh et al. [11] have suggested that the jitter velocity (i.e. the linearized velocity response to the applied oscillating electric field) of the ions in the oscillating radial electric field near the Faraday screen may directly give rise to sputtering in some cases. Recently, Perkins [12] has investigated the role of the RF sheath near a Faraday shield element, noting particularly the enhancement of the oscillating RF electric fields and hence the ion jitter velocities in the sheath.

The present paper builds on the model of Perkins [12], with emphasis on a complementary regime of ion dynamics in which the ions are strongly magnetized and rectification effects in the oscillating sheath play a more dominant role. The rectification of the applied ICRF by the sheath leads to the development of a DC potential drop which, acting in combination with the conventional Debye-Bohm sheath, accelerates ions into the surface of the Faraday screen.

This extension to the model of Perkins is important, for several reasons. First, as we shall see, experiments often lie in a range where the ions are neither completely unmagnetized (as in the model of Perkins) nor completely magnetized (the present model). Since this intermediate regime is difficult to treat, it is important to understand the physics of both limiting cases. In this regard, the present model is also important as a benchmark case for particle simulations of the sheath problem. Second, in contrast to Ref. [12], the present model allows the ions to impact the surface of the Faraday screen at grazing angles of incidence, where sputtering yields are potentially much larger than for normal incidence. Finally, the strongly magnetized regime that we treat here will turn out to be the one that applies in the limit of low plasma density at the Faraday screen, where we propose operation in order to minimize the impurity influx.

Unlike the Puri model, the RF sheath mechanisms described here and in Ref. [12] do not require ion cyclotron resonance of an impurity or primary species with the RF field. Consequently, the RF sheath tends

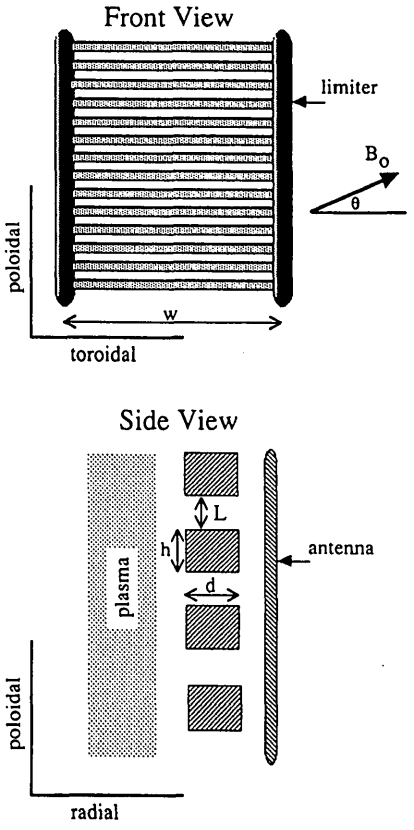

FIG. 1. Schematic illustration of the Faraday screen and antenna geometry for fast wave excitation in a tokamak.

to be robust and operative over a wide range of plasma and wave field conditions. Nevertheless, there is as yet no experimental reason to exclude resonant mechanisms and, in fact, the sheath mechanism which we describe could well operate in conjunction with them.

The physics of RF sheaths has been studied by previous authors in other contexts, and a growing literature of both experimental [14-16] and theoretical [17-20] papers exists. A unique feature of the Faraday screen ICRF sheath is the presence and orientation of the tokamak DC magnetic field relative to the Faraday screen elements. Indeed, this orientation was found to have an important impact on the observed impurity concentrations [21]. In addition to affecting the coupling of the antenna to the slow wave, the relative orientation of the DC magnetic field and the Faraday screen surface is an important parameter in the RF sheath models to be discussed subsequently.

Although the RF sheath mechanism discussed here applies to both fast wave (FW) and ion Bernstein wave (IBW) antennas, we will restrict discussion here to the FW antenna. The Faraday screen and the antenna geometry for FW excitation in a tokamak are illustrated schematically in Fig. 1. The orientation angle θ

is typically about 10° for the FW case. For simplicity, we consider in this paper the idealized limit of identical rectangular cross-section elements with $d \gg L$ and $w \gg L/\sin\theta$, so that the RF sheaths between adjacent Faraday screen elements may be modelled as the one-dimensional problem of a plasma filled capacitor, with the poloidal direction being the non-ignorable one.

Since, in practice, almost all of the RF magnetic flux from the antenna links the Faraday screen, the entire voltage across the antenna V_a must appear across the Faraday screen, and the voltage induced across adjacent elements is $V = V_a/N$, where N is the number of Faraday screen gaps. This voltage is the drive for the RF sheath. In this paper, we have in mind the situation where $eV \gg T_e$. In the absence of plasma sheath effects (e.g. in the vacuum limit) the electric field in the gap is V/L, which is larger than the electric field near the antenna by the factor (L+h)/L. Sheath effects increase this factor to (L+h)/Δ, where Δ is the RF sheath width defined by Eqs (1) or (2) in Section 2. This larger electric field is sustained by induced surface charges. The plasma response to the voltage drive will be treated in the electrostatic approximation under the assumptions that $N(h+L) \ll c/\omega$, $w \ll c/\omega$ and $(L+h) \gg \Delta$.

In Section 2, the regimes of electron and ion response in the sheath and presheath are delineated. The phenomenon of rectification is discussed. Regime diagrams are given for typical FW tokamak experiments. Further details of sheath physics, including electron heating and a discussion of ion orbits in various regimes, can be found in a companion report [22]. A numerical model of the sheath is given in Section 3 for one regime of particular interest: cold, immobile, magnetized fluid ions and magnetized electrons which satisfy the Maxwell-Boltzmann relation. The transition from the vacuum limit to the fully shielded plasma limit is discussed and it is shown that the plasma density is a key parameter. Some implications of the model for ICRF experiments are discussed in Section 4. The sputtering rates due to ion acceleration in the rectified fields are estimated. The feasibility of reducing sputtering by operation with low densities at the Faraday screen is considered with a view to maintaining good ICRF coupling. Finally, Section 5 presents our conclusions.

2. RF SHEATH REGIMES

In this section, various regimes of RF sheath operation are qualitatively discussed, with physical arguments presented at an order of magnitude level of accuracy. We shall return to a more mathematically precise description of one regime of particular importance in Section 3. The one-dimensional capacitor sheath model employed here is illustrated schematically in Fig. 2.

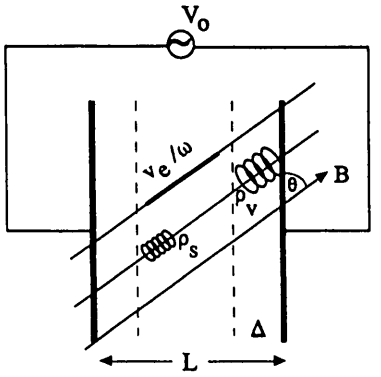

FIG. 2. One-dimensional model of the plasma-filled capacitor sheath, showing the plate separation L, the sheath width Δ, the thermal electron excursion in a wave period v_e/ω, and the characteristic ion Larmor radii in the presheath and sheath, ρ_s and ρ_v, respectively. The applied voltage is V_0 and B is the equilibrium magnetic field.

The gap region of total length L typically contains a non-neutral RF sheath region of width Δ adjacent to each plate. The sheath contains mainly ions; its width can be estimated from Poisson's equation as $V/\Delta^2 \approx 4\pi e n_{is}$ where n_{is} is the local density in the sheath. This density can be estimated from the steady state continuity equation if the ion flow velocity is known. For simplicity, in the following discussion we restrict our attention to the case of cold fluid ions. When both the sheath and presheath ions are magnetized (i.e. $\rho/\Delta \ll 1$ and $\rho/L \ll 1$, as discussed subsequently), the characteristic ion flow velocity in the presheath is the sound speed c_s defined by $c_s = (T_e/m_i)^{1/2}$. The flow is predominantly parallel to the magnetic field, thus the x component of velocity (i.e. normal to the plates) is $c_s \sin\theta$. In the sheath, the ions are accelerated through a potential difference of order of magnitude V — the applied RF voltage — and hence achieve a characteristic flow velocity in the x direction of $c_v \sin\theta$, where $c_v = (eV/m_i)^{1/2}$. Thus the density in the sheath is approximately related to the density in the presheath n_{i0} by $n_{is}/n_{i0} \approx c_s/c_v$. Combining this with Poisson's equation yields the well known Child-Langmuir law for the sheath width Δ,

$$\Delta \approx \Delta_m \equiv \lambda_{De} (eV/T_e)^{3/4} \qquad (1)$$

where the symbol Δ_m denotes that the sheath and presheath are fully magnetized and λ_{De} is the Debye length. This is the same result as is obtained for a plasma without a magnetic field.

The sheath width Δ will have a different form when the ions are magnetized in the presheath but unmagnetized in the sheath. In this case, $n_{is}/n_{i0} \approx c_s \sin\theta/c_v$. Denoting the resulting sheath width by Δ_u, Poisson's equation yields

$$\Delta \approx \Delta_u \equiv \lambda_{De} (eV/T_e)^{3/4} \sin^{-1/2}\theta \quad (2)$$

A critical parameter in the study of the Faraday screen sheath is Δ/L. At high plasma density, when $\Delta/L \ll 1$, the plasma is able to shield the applied RF voltage from the presheath region, so that the electric field is small across most of the gap, and the voltage drop occurs primarily near the plates. In this limit the plasma is approximately quasi-neutral, except in sheaths where $n_{es} \ll n_{is}$. The boundary condition of zero time-averaged current to the plates constrains the structure of the self-consistent potential Φ, which adjusts to confine the bulk of the electrons away from the plates. This is accomplished for electrons satisfying the Maxwell-Boltzmann relation, $n_e \propto \exp(e\Phi/T_e)$, when Φ is at least T_e above the maximum applied potential at either plate. A well known consequence of this is a rectification effect, since the time averaged potential $\langle\Phi\rangle$ is always positive in the gap but zero at each plate (assuming an AC driving voltage). This rectified DC field gives the ions a potential hill to fall down and is the important source of ion energy for sputtering in this paper.

In the opposite limit, $\Delta/L \approx 1$, which occurs at low plasma density, the plasma is unable to effectively shield the applied RF voltage and the system begins to approach the vacuum limit. The potential need no longer provide as much electron confinement. Zero time averaged current to the plates can still be obtained because $n_e < n_i$ is permitted throughout the entire gap. In this regime the rectification effects are dramatically reduced, and with them the acceleration mechanism for RF induced ion sputtering. This suggests the possibility of enhancing the performance of ICRF Faraday screens with respect to impurity production, by reducing the local ion density at the screens. This point will be discussed in greater detail in subsequent sections.

The species responses to the sheath and presheath electric fields are governed by the ratio of $\partial/\partial t$ to $\vec{v}\cdot\nabla$ in the respective Vlasov or fluid equations. A subdivision into sheath and Bohm-presheath regions is made in the analysis. We first consider the electrons, which are always strongly magnetized in each region for parameters of interest. When

$$\omega\Delta < v_e \sin\theta \quad (3)$$

where $v_e = (T_e/m_e)^{1/2}$, the electrons satisfy the Maxwell-Boltzmann relation across the sheath. In the opposite limit, they are subject to Fermi acceleration [17, 18, 23] by the sheath front which moves at a velocity $\omega\Delta/\sin\theta$ in the x direction. The electrons will satisfy the Maxwell-Boltzmann relation across the presheath if

$$\omega L < v_e \sin\theta \quad (4)$$

However, the electron response in the presheath will not turn out to be critical in the present analysis because the electric fields in the presheath are small compared to those in the sheath. It has been shown [22] that condition (4) is unimportant when $\tilde{n}_i \ll \bar{n}_i$, where $\tilde{n}_i$ and $\bar{n}_i \equiv \langle n_i\rangle$ are respectively the fluctuating and time averaged ion densities. This inequality is satisfied in many situations of interest, including the case $\rho_s \ll L$, to be discussed subsequently. Note that the right hand side of Eqs (3) and (4) can be interpreted as the electron thermal speed with an effective mass $m_e^* = m_e/\sin^2\theta$.

The response of ions is more complicated than that of electrons, even for the cold fluid ion model which we now consider. In the presheath, the characteristic ion scale length is the Larmor radius based on the sound speed, $\rho_s = c_s/\Omega_i$. In the sheath, the characteristic ion scale length is $\rho_v = c_v/\Omega_i$. The ion response will be magnetized or not, depending on the ratio of the relevant ρ to the relevant spatial scale Δ or L. For all situations of practical interest here, the ions are strongly magnetized in the presheath because

$$\rho_s \ll L \quad (5)$$

In contrast, both magnetized and unmagnetized limits are possible for the ions in the sheath. Under the condition that

$$\Delta_u \ll \rho_s \quad (6)$$

the sheath is completely unmagnetized and is separated from the Bohm presheath by a wide magnetic presheath of width ρ_s. This situation has been discussed in the literature for the DC sheath problem [24]. The structure of the magnetic presheath when $\theta \ll 1$ is considered in the companion report [22]. The function

of the magnetic presheath is to accelerate the ions from a velocity $c_s \sin\theta$ at the Bohm presheath to c_s (as required by the Bohm sheath condition) at the sheath entrance.

More typically, for ICRF Faraday shield parameters $\rho_s \ll \Delta_u$, and the interesting comparison is of ρ_v with Δ_u or Δ_m. When

$$\rho_v \ll \Delta_m \tag{7}$$

it is to be expected, and will be shown subsequently, that the sheath ions obey a strongly magnetized limit of the equations in the sheath and their motion is dominated by parallel flow along the field lines. If neither Eq. (6) nor Eq. (7) is satisfied, then the ions will have complicated orbits in some region (sheath or magnetic presheath). When

$$\rho_v \gg \Delta_u \tag{8}$$

the ion motion is, to a good approximation, unmagnetized in the sheath itself. Note also that for small θ a complicated transition regime exists in which $\Delta_m < \rho_v < \Delta_u$, where the sheath ions are neither magnetized or unmagnetized.

Figure 3 shows the most important of these regime boundaries for present day fast wave experiments. Specifically, we consider typical JET [1] FW parameters, with V = 500 V, f = 30 MHz (applied ICRF frequency), L = 5 mm and $\theta = 10°$. At $T_e = 30$ eV and $n_{i0} = 10^{11}$ cm^{-3}, the plasma shielding is effective ($\Delta_m/L \ll 1$), the Maxwell-Boltzmann approximation for the electrons is marginal in the sheath, and the ions are fully magnetized in the sheath and presheath. Typically, a magnetized ion model should be good at low densities and is useful for studying the transition from a shielded regime to a vacuum regime. Conversely, an unmagnetized ion sheath model is appropriate at the higher densities.

To elucidate the ion dynamics further, we consider the solution for the ion density in the cold fluid model:

$$\frac{\partial n_i}{\partial t} + \nabla\cdot(n_i\vec{u}) = S \tag{9a}$$

$$\frac{\partial \vec{u}}{\partial t} + \vec{u}\cdot\nabla\vec{u} = \frac{q}{m}\vec{E} + \frac{q}{mc}\vec{u}\times\vec{B} \tag{9b}$$

where S is a particle source, $\vec{u}$ is the ion fluid velocity and, in the one-dimensional model, $\vec{E} = \hat{e}_x E$, $\nabla = \hat{e}_x\,\partial/\partial x$ and $\vec{B} = B_x\hat{e}_x\cos\theta + B_z\hat{e}_z\sin\theta$.

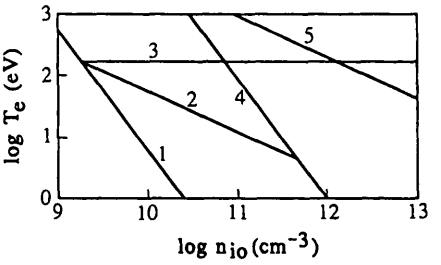

FIG. 3. Important regime boundaries for the RF sheaths in typical ICRF heating experiments. Here we consider FW excitation for typical JET parameters: V = 500 V, f = 30 MHz, L = 5 mm and $\theta = 10°$. The expected temperature and density at the Faraday screen are $T_e \sim 30$ eV and $n_{i0} \sim 10^{11}$ cm^{-3}, with large uncertainties. In the region above and to the right of curve 1, the applied voltage is fully shielded ($\Delta < L$). Above curve 2, the condition for Maxwell-Boltzmann electrons is satisfied in the sheath ($\omega\Delta < v_e \sin\theta$). Above curve 3, the condition for Maxwell-Boltzmann electrons is satisfied in the presheath ($\omega L < v_e \sin\theta$). Below curve 4, the ions are magnetized or equivalently immobile in the sheath ($\rho_v < \Delta$). Above curve 5, the ions are fully unmagnetized in the sheath ($\rho_s > \Delta$).

Eliminating the other velocity components in favour of u_x, Eq. (9b) can be cast into the form

$$D^3u_x + Du_x = D^2v_x + v_x\sin^2\theta \tag{10}$$

where

$$D = \frac{1}{\Omega_i}\left(\frac{\partial}{\partial t} + u_x\frac{\partial}{\partial x}\right) \equiv D_t + D_x \tag{11a}$$

$$v_x = \frac{qE_x}{m\Omega_i} \tag{11b}$$

In the unmagnetized limit, $\rho/\ell \gg 1$, where ρ and ℓ are typical gyroradii and scale lengths, D may be approximated by $D_x \gg 1$, and Eq. (10) reduces to

$$D_x^3\,u_x = D_x^2\,v_x \tag{12a}$$

or

$$\frac{\partial}{\partial x}\left(\frac{1}{2}u_x^2 + \frac{q\Phi}{m_i}\right) = 0 \tag{12b}$$

In this limit, the ions respond to the instantaneous potential Φ. There is a large component of this AC

jitter velocity normal to the plates. This limit is essentially the one treated by Perkins [12].

In the opposite limit, $\rho/\ell \ll 1$, we have $D_x \ll D_t \sim O(1)$ since $\partial/\partial t \sim \Omega_i$. An instructive ordering in this limit is to take $\sin\theta \approx \theta \sim \rho/\ell$ and to expand u_x in even powers of ρ/ℓ

$$u_x = u_0 + u_2 + \ldots \tag{13}$$

Each component of u is split up into fluctuating and time averaged parts, so that $u_0 = \bar{u}_0 + \tilde{u}_0$, with $\langle\tilde{u}_0\rangle = 0$ and $\bar{u}_0 = \langle u_0\rangle$, where $\langle\,\rangle$ is a time average over an RF cycle.

In leading non-trivial order [$\sim(\rho/\ell)^0$], Eq. (10) yields

$$D_t^2\,\tilde{u}_0 + \tilde{u}_0 = D_t\tilde{v}_0 \tag{14a}$$

which gives the leading order $\tilde{u}_x$ as

$$\left(\frac{\partial^2}{\partial t^2} + \Omega_i^2\right)\tilde{u}_x = \frac{q}{m}\frac{\partial E_x}{\partial t} \tag{14b}$$

where $v_x \equiv \tilde{v}_0 + \bar{v}_0$. The next non-trivial order [order $(\rho/\ell)^2$], yields the constraint equation determining $\bar{u}_0$,

$$\langle(\tilde{D}_x D_t^2 + D_t^2\tilde{D}_x + \tilde{D}_x)\,\tilde{u}_0\rangle + \bar{D}_x\bar{u}_0 = \langle\tilde{D}_x D_t\tilde{v}_0\rangle + \bar{v}_0\sin^2\theta \tag{15}$$

where we have defined $\tilde{D}_x = (\tilde{u}_x/\Omega_i)(\partial/\partial x)$ and $\bar{D}_x = (\bar{u}_x/\Omega_i)(\partial/\partial x)$. In obtaining Eq. (15) we have noted that $D_t \sim (\rho/\ell)^0$, $\tilde{D}_x \sim (\rho/\ell)^2$, $\bar{D}_x \sim (\rho/\ell)\theta \sim (\rho/\ell)^2$. After some manipulations of Eq. (15) which involve parts integration in time using Eq. (14), some cancellations occur, leaving a simple result for the leading order $\bar{u}_x$:

$$\frac{\partial}{\partial x}\left(\frac{1}{2}\bar{u}_x^2 + \frac{q\langle\Phi\rangle}{m_i}\sin^2\theta\right) = 0 \tag{16}$$

Equation (16), derived here for the ordering $\theta \sim \rho/\ell$, can also be shown to be valid for $\sin\theta$ of order unity, provided $\rho/\ell \ll 1$. Thus, in the magnetized limit $\rho/\ell \ll 1$, the ions have an AC jitter velocity with a substantial component normal to the plates, $\tilde{u}_x \simeq \tilde{u}_0$, given by Eq. (14), and a DC flow component along the field lines, $\bar{u}_\parallel \equiv \bar{u}_x/\sin\theta$, given by Eq. (16). In order of magnitude in the sheath, we have $\bar{u}_\parallel \sim c_v$, while $\tilde{u}_x \sim c_v\,(\rho_v/\Delta) \ll \bar{u}_\parallel$. The above ordering is valid for small θ, provided $\theta \gg (\rho/\ell)^2$, otherwise additional correction terms appear in Eq. (16).

The energy of ions striking the plate is dominated by the DC flow when $\rho_v/\Delta \ll 1$ since $\bar{u}^2 \gg \tilde{u}^2$; however, the angle at which the ions hit the plate can be significantly affected by the AC jitter. We denote the angle of the ion trajectory to the surface by ψ, with $\psi = \pi/2$ corresponding to normal incidence. Then, $\tan\psi = u_x/(u_y^2 + u_z^2)^{1/2} \approx u_x/u_\parallel$, and for small angles we find

$$\psi \simeq \theta + \frac{\tilde{u}_x}{\bar{u}_\parallel} \tag{17}$$

where $\tilde{u}_x$ must be evaluated at the time of impact and $\tilde{u}_x/\bar{u}_\parallel \sim \rho_v/\Delta \ll 1$. Equation (17) can be important when $\theta \sim \rho_v/\Delta$, since the sputtering yields are very sensitive to angle for small angles. In the case where $\theta < \rho_v/\Delta < \theta^{1/2}$, a distribution of impact angles results, with $\psi \sim (\theta\rho_v/\Delta)^{1/2}$, as shown in the Appendix.

Given the solution for $\tilde{u}$ in the $\rho/\ell \ll 1$ and $\rho/\ell \gg 1$ regimes, n_i can be determined by Eq. (9a). Considering $\rho/\ell \gg 1$ first, the $\partial n_i/\partial t$ term is negligible, and we have

$$\frac{\partial}{\partial x}(n_i u_x) = S \tag{18}$$

where the instantaneous u_x is obtained from Eq. (12b).

In the $\rho/\ell \ll 1$ regime, Eq. (9a) can be time averaged to yield

$$\frac{\partial}{\partial x}(\bar{n}_i\bar{u}_x + \langle\tilde{n}_i\tilde{u}_x\rangle) = \langle S\rangle \tag{19a}$$

where $\bar{u}_x = \bar{u}_\parallel \sin\theta$. Equation (9a) can be used in its unaveraged form to show that $\tilde{n}_i/\bar{n}_i \sim (\rho/\ell)^2 \ll 1$, so that Eq. (19a) reduces to an equation for $\bar{n}_i$:

$$\frac{\partial}{\partial x}(\bar{n}_i\bar{u}_x) = \langle S\rangle \tag{19b}$$

Evidently, when Eq. (16) is valid, the flux to the plate is dominated by the DC contribution $\bar{n}_i\bar{u}_x$, not by $\langle\tilde{n}_i\tilde{u}_x\rangle$. Thus, the validity condition for Eq. (16), $(\rho/\ell)^2 \ll \sin\theta$, also ensures that the Child-Langmuir form for the sheath width, Eq. (1), applies.

3. NUMERICAL MODEL OF THE SHEATH FIELDS

The simplest model which is relevant to our present interests is one consisting of cold fluid, fully magnetized ions and Maxwell-Boltzmann electrons in both the sheath and the presheath. In Fig. 3 it is shown that these approximations should be qualitatively valid at low densities and high electron temperatures. Some previous work [17-19] has focused on essentially this description. Lieberman [19] has extended a very useful qualitative model introduced by Godyak [18] to obtain solutions in the fully shielded regime $\Delta \ll L$. Closed form analytical estimates of various sheath quantities are given in the large eV/T_e limit.

For the Faraday screen application, our main interest is in determining the rectification and the ion energy available for sputtering as a function of plasma density, with particular attention to the plasma-vacuum transition which occurs when $\Delta \sim L$. The practical question we wish to address is whether substantial improvement in high-Z impurity generation at the Faraday screen can be achieved by operation in the low density $\Delta \sim L$ regime. This necessitates a numerical treatment.

The model equations we consider are as follows:

$$n_e = n_{ec}(t) \exp(e\phi/T_e) \tag{20}$$

$$n_i = \frac{n_{i0}}{[1+2e(\langle\Phi_0\rangle - \langle\Phi\rangle)/m_i u_0^2]^{1/2}} \tag{21}$$

$$\frac{\partial^2\Phi}{\partial x^2} = -4\pi e(n_i - n_e) \tag{22}$$

where n_{i0} (independent of space and time) is the specified ion density of singly charged ions ($q=e$) at the system midplane $x = x_0$, $\Phi_0 \equiv \Phi(x_0)$, and u_0 is a specified flow velocity of particles ejected parallel to the B field at the location of the source $x=x_0$. We make the restriction $u_0 \geq c_s$, to satisfy the usual Bohm condition. Equation (21) follows from Eq. (16) by employing the time averaged continuity equation (19b) in the source-free regions to the right and left of $x=x_0$. The boundary conditions on Eqs (20)-(22) are as follows:

$$\Phi(x_1) = V_1 \tag{23a}$$

$$\Phi(x_2) = V_2 \tag{23b}$$

$$\frac{\partial}{\partial t}[E(x_2) - E(x_1)] = 0 \tag{24}$$

$$\langle J_{i1} + J_{e1}\rangle = 0 \tag{25}$$

where $V_1 = (V_0/2)\cos(\omega t)$ and $V_2 = -(V_0/2)\cos(\omega t)$ are the applied voltages at the left ($x=x_1$) and right ($x=x_2$) plates. Equation (24) follows from the Gauss law, noting that in the strongly magnetized limit the displacement current dominates the particle conduction current. In Eq. (25), the ion and electron current densities projected along a field line impacting the plate at $x=x_1$ are

$$J_{i1} = n_{i0}\, e\, u_0 \tag{26}$$

$$J_{e1} = -\frac{ev_e}{\sqrt{2\pi}} n_{ec} \exp(eV_1/T_e) \tag{27}$$

where $v_e = (T_e/m_e)^{1/2}$ is the electron thermal velocity.

It will be noted that Eqs (20)-(27) contain no explicit reference to the magnetic field angle θ, since both electrons and ions are in the strongly magnetized limit. Thus, the model system is identical to that which is obtained in the absence of a magnetic field. The dimensionless variables and the input parameters which characterize the problem are: variables $\Psi(\xi, \tau) \equiv e\Phi/T_e$, $\xi \equiv x/\lambda_D$, where $\lambda_D \equiv (T_e/4\pi n_{i0}e^2)^{1/2}$, $\tau \equiv \omega t$, $\eta(\tau) \equiv n_{ec}/n_{i0}$; and parameters $u_{cs0} \equiv u_0 (m_i/T_e)^{1/2}$, $\Psi_0 \equiv eV_0/T_e$, m_i/m_e and L/λ_D, where $L = |x_2 - x_1|$ is the system length.

The equations and constraints (20)-(27) are differential in space and integral in time. By discretizing the time variable into N_t time points on the domain $0 \leq \tau \leq \pi$ and performing the integrations using Simpson's rule, the problem may be cast into a high order, non-linear, ordinary differential, boundary value problem. This problem, while complex, is of a type that can be solved by the general purpose boundary value code COLSYS [25]. In the strongly magnetized limit, $c_v/\omega\Delta \ll 1$, $c_s/\omega L \ll 1$, of interest here (sometimes referred to as the 'immobile ion' limit, since the ions have sufficient inertia to be effectively immobile in the AC fields), the numerical procedure just described is much more efficient than direct numerical integration of the ion fluid equations. This is because the direct method requires following the evolution over many RF cycles until the system relaxes to a periodic state.

Output for a typical code run is shown in Fig. 4, for the case $n_{i0} = 1\times10^{11}$ cm^{-3}, $V_0 = 500$ V,

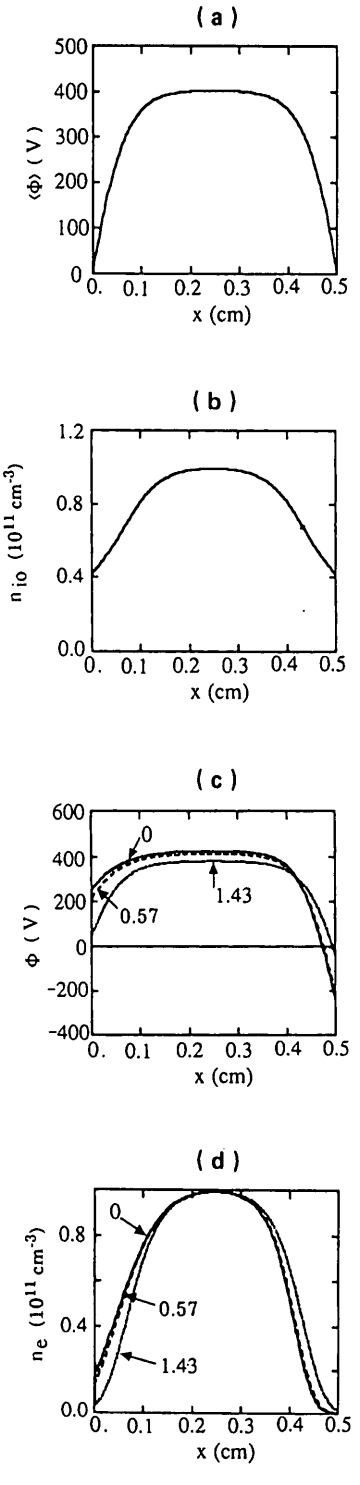

FIG. 4. Output for a typical code run for the case $n_{i0} = 1 \times 10^{11}$ cm^{-3}, $V_0 = 500$ V, $m_i/m_e = 3672$, $L = 0.5$ cm, $T_e = 100$ eV, $u_{cs0} = 1.3$ and $N_t = 12$. (a) Time averaged potential $\langle\Phi\rangle$ as a function of distance x across the gap. (b) Ion density n_{i0}, which is independent of time in this model. (c) Potential Φ as a function of x at the times $\tau = \omega t = 0$, 0.57 and 1.43, corresponding approximately to $\tau = 0$, $\pi/4$ and $\pi/2$. Note than Φ_0 always exceeds the applied voltage at either plate. (d) Electron density n_e as a function of x at the same times as in (c).

$m_i/m_e = 3672$, $L = 0.5$ cm, $T_e = 100$ eV, $u_{cs0} = 1.3$ and $N_t = 12$. The time averaged potential $\langle\Phi\rangle$ in Fig. 4(a) results from a combination of the usual Debye-Bohm sheath with the expected sheath rectification effect of the applied AC voltage, as described in Section 2. The ion density, independent of τ in this model, is shown in Fig. 4(b). Figure 4(c) shows the potential as a function of space at various times, corresponding approximately to $\tau = 0$, $\pi/4$ and $\pi/2$. Note that Φ_0 always exceeds V_1 and V_2, as is required for electron confinement. This is the fundamental origin of the observed rectification. Figure 4(d) shows the electron density n_e at the same times. The electrons slosh back and forth in the gap, strongly avoiding the sheath at the low potential side. The DC potential drop seen by the ions in this example is $\langle\Phi_0\rangle = 403$ V. For an ion in charge stage Z, the resulting energy available for sputtering, $Ze\langle\Phi_0\rangle$, is therefore well in excess of the sputtering thresholds, and is a good candidate mechanism for explaining the experimental observations.

Some of the detailed behaviour observed with the code can be understood analytically in limiting cases. For example, in the limit $eV/T_e \gg 1$ and $\Delta \ll L$, there is an analytical expression for the time dependence of Φ_0. Using the fact that $d\Phi/dx$ is proportional to $(\Phi_0 - \Phi)^{1/4}$ for a Child-Langmuir sheath, and combining Eqs (23) and (24), it can be shown that

$$(\Phi_0 - \tfrac{1}{2} V_0 \cos \omega t)^{1/4} + (\Phi_0 + \tfrac{1}{2} V_0 \cos \omega t)^{1/4} = V_0^{1/4} \quad (28)$$

The DC potential drop $\langle\Phi_0\rangle$ available for sputtering is considered for a range of densities and temperatures in Fig. 5. Parameters other than n_{i0} and T_e are the same as in Fig. 4. At the high density end of this plot, $\langle\Phi_0\rangle$ saturates because $\Delta \ll L$. The saturated value is larger for the $T_e = 100$ eV case than for the $T_e = 30$ eV case because of the correspondingly larger DC Debye-Bohm sheath.

The model used to compute Fig. 5 is not obvisously valid in the extreme high and low density limits but turns out to be a good approximation in these limits, for the following reasons. At high densities, Δ becomes sufficiently small that the $\rho_v/\Delta < 1$ expansion becomes suspect, but the curves in Fig. 5 attain their asymptotic values before this occurs. As the density is lowered, Δ increases and, eventually, condition (3) is no longer satisfied at fixed T_e. To test the sensitivity of our conclusions in the face of this deficiency, a density scan was also made, with T_e raised, if neces-

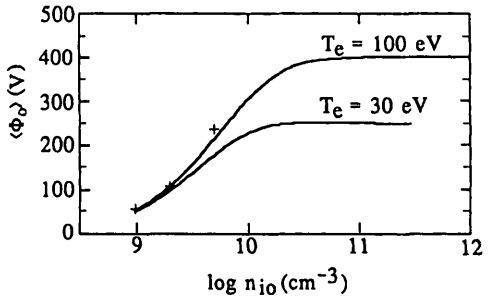

FIG. 5. DC potential drop $\langle\Phi_0\rangle$ available for sputtering versus presheath ion density. Parameters other than n_{i0} and T_e are the same as in Fig. 4. The data points at low densities indicated by the 'plus' symbol were obtained by choosing T_e such that $\omega\Delta \geq v_e \sin\theta$.

sary, at each density so that $\omega\Delta \leq v_e \sin\theta$ pertained. The physical justification for this is Fermi acceleration of the electrons by the moving sheath front [19, 22, 23]. The resulting data points are shown by the 'plus' symbols in the figure. Figure 5 shows that the details of the electron model are not critical in the low density regime because the plasma ceases to be quasi-neutral there ($n_e \ll n_i$).

With regard to the problem of impurity generation, Fig. 5 is of interest, for two reasons. First, it shows that the rectification and hence ion sputtering can be reduced at low sheath densities. Second, it indicates a range of variation of $\langle\Phi_0\rangle$, which is important information since the local density and temperature at the Faraday screen of a powered antenna are not known experimentally and are difficult to measure.

4. DISCUSSION AND APPLICATION OF THE MODEL TO ICRF EXPERIMENTS

4.1. Estimate of the impurity influx

In the magnetized ion model discussed in the previous section, sputtering occurs when ions of charge Ze fall down the rectified DC potential, gaining an energy $Ze\langle\Phi\rangle$. It is evident that for the RF parameters of Fig. 5 and at Faraday screen densities exceeding about 10^{10} cm^{-3}, energies in excess of a few hundred eV are available for sputtering, even for a singly charged ion species. The relevant species are the deuterium majority ions, light impurities such as carbon and oxygen, and the Faraday screen material itself. For normal incidence ($\psi = 90°$) of a deuterium projectile on a nickel target, the yield [13] is of order $Y \approx 0.04$ when the incident energy is between 300 and 2000 eV. Y varies from 0.4 to 0.9 for carbon on nickel and from 0.5 to 2.0 for nickel on nickel over the same energy range. Evidently, the parameters of the RF sheath are conducive to efficient physical sputtering, especially by impurity ions. Furthermore, sputtering yields are generally not maximized at $\psi = 90°$. For deuterium on nickel the maximum occurs approximately at $\psi = 10°$, while for nickel on nickel the maximum occurs approximately at $\psi = 30°$ [13]. At their maximum as a function of angle, the yields are typically enhanced by a factor of two to five over normal incidence. These data are for clean smooth surfaces. The effect of surface roughness has been examined by fractal methods [26] and may be a quantitatively important correction in some cases. Sputtering data for chromium — the influx actually measured in the JET experiments [1, 27] — are the same as those for nickel within measurement and modelling errors, as far as such data are available. Thus the two materials will be treated interchangeably in the following discussion.

For the case of nickel on nickel, the yields can easily exceed unity. Even at normal incidence this occurs when the incident energy is above about 500 eV. If neutral nickel sputtered from a nickel surface were adequately confined in the vicinity of the sheath, it could be ionized (perhaps even several times) and be available for resputtering. The possibility of a cascade or avalanche under some operating conditions is evident. In this regard, nickel is a poor Faraday screen material; carbon and beryllium, which have lower self-sputtering yields, are superior.

For JET, assuming a density at the Faraday screen of $n_{i0} = 10^{11}$ cm^{-3}, $T_e = 30$ eV and a gap voltage $V_0 = 500$ V (consistent with operation at the highest powers of about 2 MW per Faraday screen), we have $\langle\Phi_0\rangle = 250$ V (Fig. 5). The expected impurity influx measured in front of the Faraday screen can be estimated from

$$\Gamma_I = Y(\psi)\, R\, n_{i0}\, c_s \sin\theta \qquad (29)$$

where the factor $R \approx 0.2$ is the ratio of Faraday screen area in which sputtering occurs (between the gaps) to the area of the entire front face of the screen (gaps plus elements). Assuming $\theta = 10°$ and estimating $\psi = 30°$ from Eq. (17), the sputtering yield for deuterium on nickel is $Y_D = 0.1$ and the yield for carbon on nickel is $Y_C = 2.1$, where we assume a typical charge state of $Z = 3$ for carbon ions which

diffuse to the screen from the SOL and estimate $Y(\psi)/Y(90°) = 3$ for both species. Therefore, the nickel influx due to sputtering by deuterium is found from Eq. (29) to be $\Gamma_I(D) \approx 1\times10^{15}$ atoms·cm^{-2}·s^{-1}. If we assume that the local carbon density is about 30% of the deuterium density near the antenna (for antennas with graphite protection tiles), the nickel influx due to sputtering by carbon can be estimated as $\Gamma_I(C) \approx 6\times10^{15}$ atoms·cm^{-2}·s^{-1}. Therefore, the total nickel influx neglecting self-sputtering is approximately 7×10^{15} atoms·cm^{-2}·s^{-1}, a result comparable in order of magnitude to the maximum observed impurity influx [27] of $\Gamma_I \approx 10^{16}$ atoms·cm^{-2}·s^{-1} on JET.

The important conclusion which can be drawn from the preceding estimates is that sputtering by heavy ions accelerated in a typical RF sheath can provide a satisfactory explanation of the magnitude of the observed impurity influx. The physical reason why heavy ions must be included in the metal impurity generation model is that the sputtering coefficient Y is intrinsically larger for heavier projectiles. In addition to sputtering by carbon, self-sputtering by the Faraday screen material may also play a significant role at high edge density. Detailed models of these processes are needed which include self-consistent estimates of the densities of the various ion species. Since such a model requires a treatment of ionization and transport between the SOL and the Faraday screen gaps, it is outside the scope of the present paper, but these considerations are being examined in detail in a separate study [9].

4.2. Scaling of the impurity influx

In addition to the obvious scalings of Γ_I in Eq. (29), the RF sheath model gives implicit dependences of Y on density and angle which are rather complicated. With regard to density, Fig. 5 illustrates that the increase in sputtering energy, and hence Y, with n_{i0} is an important effect at low density. Also, the decrease of the sheath width with increasing density means that the unmagnetized sheath regime is approached and the impact angle ψ approaches 90° as n_{i0} increases, leading to a significant decrease in $Y(\psi)$. Thus, the apparent linear increase in Γ_I with n_{i0} is supplemented by the former effect and partially offset by the latter. Even neglecting the physics of self-sputtering, which depends on density through ionization rates, it is obvious that the density scaling of Γ_I may deviate from linear scaling and is different at low and high density.

The θ dependence in Eq. (29) also deserves comment. First, we note an important technical point which follows from the discussion preceding Eq. (2): the factor of $\sin\theta$ belongs in Eq. (29) even in the unmagnetized *sheath* limit ($\rho_v \gg \Delta$) because the Bohm *presheath*, where n_{i0} is evaluated, is always magnetized ($\rho_s \ll L$) for parameters of interest. (The $\sin\theta$ factor is not accounted for in the fully unmagnetized ion simulations of Ref. [12], which therefore tend to overestimate Γ_I.) In this regime, the $\sin\theta$ factor is the dominant angular dependence and alignment of the screen with the field lines can greatly reduce the impurity influx from gap sheaths. However, RF sheaths in locations other than in the gaps (e.g. on the front face of the screen or between the screen and the protection tiles) may also occur. The θ dependence of these sheaths is not correctly described in a one-dimensional model.

The wealth of data on the scaling of central impurity accumulation with tokamak density (which influences n_{i0}), plasma current (which controls θ and hence influences ψ) and RF power (which influences V and n_{i0}) invites comparison with the present model. However, there are at least three difficulties in attempting this comparison. First, the density n_{i0} required by the sheath theory is not the SOL density usually measured, but the density at the Faraday screen, which depends sensitively on the details of the transport in front of the antenna. The second difficulty is that the phenomenon of impurity screening [28] by ionization in the SOL and parallel flow to limiters results in core impurity concentrations not being simply proportional to the local influx Γ_I calculated here. Third, resputtering of Faraday screen material from the limiters and other surfaces in the tokamak acts as an additional source of core impurities. Thus, it is only meaningful to test the present model by using local influx data.

Fortunately, some spectroscopic measurements have been made of the local influx from the Faraday screens on JET [1, 29]. An analysis of the experimental scaling of the chromium influx data from JET and a comparison with a model including both the sheath and SOL physics is reported in detail elsewhere [9]. However, we note here that the JET spectroscopic measurements of the *local influx from the screens* show the qualitative trends expected at the level of the present model, namely that the experimentally observed influx increases (non-linearly) with edge density and with antenna voltage.

4.3. Reduction of sputtering by edge density control

From Fig. 5 and Eq. (29) it is evident that a direct means of reducing sputtering is to reduce the local

density n_{i0} at the Faraday screen. If this approach is to be followed, a significant question that arises is whether the lower density is consistent with good wave coupling. For FW launch, good coupling can be maintained if the FW cut-off point is sufficiently close to the antenna. The cut-off point is the location where the local density satisfies

$$\frac{\omega^2}{\Omega_i(\omega+\Omega_i)} = \left(\frac{k_\parallel c}{\omega_{pi}}\right)^2 \tag{30}$$

Beyond the cut-off point the wave decays exponentially, with the exponential decay length approaching $1/k_\parallel$ in the vacuum limit. Thus, for good coupling the cut-off point must be much closer than $1/k_\parallel$ from the Faraday screen. Typically, this condition is not very difficult to satisfy, but if the density is also to be low at the Faraday screen, steep edge density profiles may be required (depending on the antenna $k_\parallel$ spectrum, which in turn depends on the geometry of the antenna cavity). Whether steep gradients can be maintained in the presence of transport and convection processes (enhanced by the RF [1, 30]) is still an open question. It must also be ensured that the wave energy does not reflect back towards the antenna in the steep gradient case. However, the problem of designing antenna systems with good coupling and low density at the Faraday screen does not seem insoluble, particularly in larger tokamaks such as JET and TFTR.

4.4. Limitations of the sheath model

The one-dimensional model described in our paper is probably the simplest possible model which retains the essence of the RF sheath ion acceleration mechanism. There are other sheath related physical phenomena which are not described by the present one-dimensional modelling. One such effect is that of radial ion $\vec{E}\times\vec{B}$ drifts in the sheath. These drifts can be expected to give a quantitative correction to phenomena on the time-scale for an ion to $\vec{E}\times\vec{B}$ drift radially into or out of the sheath, $\tau_{EB} = d\Delta/\rho_v c_v$. The radial dimension d is defined in Fig. 1. The parallel ion flow time through the sheath is $\tau_{\parallel s} = \Delta/c_v \sin\theta$. The neglect of $\vec{E}\times\vec{B}$ drifts on the sheath dynamics itself is therefore valid, provided that $\tau_{\parallel s} < \tau_{EB}$, which yields $\rho_v < d \sin\theta$. While this condition is typically easy to satisfy, $\vec{E}\times\vec{B}$ drifts can still compete on the slower transport-like time-scale which is required to describe the fuelling of the plasma density in the sheath.

For the sake of definiteness and clarity, we have focused our attention in this paper on the sheaths that form between individual Faraday screen elements. In a real antenna system, similar sheaths will form on any field lines that connect metal surfaces at different voltages. For antenna systems that are enclosed in a box with lateral protection tiles, sheaths between the lateral protection tiles or between the tiles and the front face of the Faraday screen are also possible. Indeed, RF enhanced impurity production from the protection tiles has been documented experimentally [31]. Front face and tile sheaths are driven by the same physics as in the present model, viz. parallel confinement of electrons on the RF sheath and slow time-scales for field lines intersecting solid surfaces.

5. CONCLUSIONS

The principal conclusion of this study is that under typical operating conditions of ICRF antennas, the RF sheath in the Faraday screen gaps is an efficient accelerator of ions for sputtering. The DC acceleration mechanism discussed here provides sufficient energy to allow both deuterium and carbon induced sputtering, and self-sputtering of the screen material, for a Faraday screen gap region with density $n_{i0} > 10^{10}$ cm^{-3}. For JET, an explanation of the observed impurity influx involves sputtering by heavy ions. An estimate of the influx based on Eq. (29) gives an order of magnitude agreement with the chromium influx data from JET [1, 27] and gives qualitative insight to guide further modelling and experiments. For a better estimate of the influx and its scaling with density, voltage and angle, further development of the model is required. Work is in progress to obtain a quantitative and self-consistent evaluation of the impurity influx by coupling the RF sheath/sputtering model to a SOL model and is reported elsewhere [9].

The sheath model of the present paper could also be improved upon in several respects. Extension of the model to include front face and tile sheaths may be critical to a complete understanding of the impurity and edge heating problems. Higher dimensional models or particle simulations (especially including the radial dimension) would enable investigation of the important question of the coupling of sheath and transport physics. Also, a full treatment of ion dynamics for the problem of a magnetized presheath and an unmagnetized sheath would be useful to understand the high density, jitter dominated RF sheath regime.

Several means of controlling RF sheath driven sputtering in FW heating experiments are available:

(1) Reducing the plasma density to the point where plasma shielding of the RF voltage is ineffective (i.e. $\Delta \sim L$) alleviates all sheath enhanced sputtering. Control of sputtering by achieving low densities locally at the Faraday screen is not necessarily bad for FW coupling, but steep edge density gradients may be required (depending on the antenna-plasma geometry) and the consistency of these with transport processes has not yet been investigated.

(2) In cases where local density control is not possible, alignment of the Faraday screen with the local magnetic field (control of θ) may be useful. For the present model of gap sheaths, screen alignment is beneficial in the high density, unmagnetized ion regime.

(3) The effective voltage driving the sheath should be reduced as much as possible. In the present model, increasing the number of elements in the Faraday screen per unit length would reduce the voltage drop per gap and hence the accelerating potential.

Appendix

ION ORBITS AND DISTRIBUTION OF ψ

In this Appendix we use Eq. (14b) to find a fairly accurate analytic expression for $\tilde{u}_x(t)$, and then find the distribution of the angle of incidence ψ, in the regime $\rho_v/\Delta < \theta^{1/2}$ where Eq. (16) is valid. As noted at the end of Section 2, Eq. (19b) implies that the sheath will have a Child-Langmuir form (see Eq. (1)) in this regime. The electric field E_x at the wall is then related to the potential drop between the plasma source and the wall, $\Phi_0 - (V_0/2)\cos\omega t$, by

$$E_x = -\frac{4}{3}\frac{[\Phi_0 - (V_0/2)\cos\omega t]^{1/4} V_0^{3/4}}{\Delta_m} \qquad (A.1)$$

Here, Φ_0 is the source potential, which in this regime may be found from Eq. (28), and Δ_m is given by Eq. (1) evaluated at V_0, i.e. $\Delta_m = \lambda_{De}(eV_0/T_e)^{3/4}$. The potential drop across the Bohm presheath, which is about T_e/e, has been neglected compared to the RF potential V, so Φ_0 is the potential at the plasma side of the Child-Langmuir sheath.

Using Eq. (28) to eliminate Φ_0, Eq. (A.1) yields

$$4(E_x/E_m - 1/2)^3 + (E_x/E_m - 1/2) + \cos\omega t = 0 \qquad (A.2)$$

where $E_m = -4V_0/3\Delta_m$. Equation (A.2), being a cubic equation, may be solved to find a closed expression for E_x. Letting $\zeta = E_x/E_m - 1/2$, we find

$$\zeta = \frac{1}{2\sqrt{3}}[(h-r)^{1/3} - (h+r)^{1/3}]$$

where $h = (1+r^2)^{1/2}$ and $r = 3\sqrt{3}\cos\omega t$. For our purposes it will be adequate to employ a Fourier expansion of the form

$$E_x = E_m(a_0 + a_1\cos\omega t + a_2\cos 2\omega t + \ldots) \qquad (A.3)$$

Since $\zeta(\omega t + \pi) = -\zeta(\omega t)$, the even coefficients must all vanish except for $a_0 = 1/2$. The odd coefficients are readily calculated numerically from

$$a_n = \frac{2}{\pi}\int_0^{\pi} d\tau\,\zeta(\tau)\cos n\tau \qquad n = 1,3,5\ldots$$

but their exact values will not be required here. The time derivative, which is needed in Eq. (14b), is

$$\frac{dE_x}{dt} = -\omega E_m(a_1\sin\omega t + 3a_3\sin 3\omega t + \ldots) \qquad (A.4)$$

yielding

$$\tilde{u}_x(t) = -\frac{4V_0\,\omega q}{3\Delta_m m_i}\left(\frac{a_1\sin\omega t}{\omega^2 - \Omega_i^2} + \frac{3a_3\sin 3\omega t}{9\omega^2 - \Omega_i^2} + \ldots\right) + A\sin\Omega_i t + B\cos\Omega_i t \qquad (A.5)$$

where A and B are constants which must be determined by the initial conditions. Note that the a_3, a_5 ... terms contribute even less to $\tilde{u}_x(t)$ than they do to dE_x/dt because the denominators, e.g. $(9\omega^2 - \Omega_i^2)$, are larger than $(\omega^2 - \Omega_i^2)$ for typical ICRF frequencies ω, which are one or two times Ω_i at the Faraday screen. Retaining only the a_1 term, Eq. (A.5) is then the solution to a simple harmonic oscillator of frequency Ω_i which is being driven at a different frequency ω. This solution for $\tilde{u}_x(t)$ is, of course, only valid near the Faraday screen surface, since the expression we used for E_x was correct near the surface. Further away from the surface, E_x will have a similar time dependence but will be smaller in magnitude.

To determine A and B, we apply the boundary condition $\tilde{u}_x = d\tilde{u}_x/dt = 0$ when $V_0 = 0$; consequently, A=B=0. Physically, by adiabatically turning on the electric field, we are keeping the driving force confined to a narrow range of frequency near ω, and the Fourier component of the driving force at frequency Ω_i is exponentially small; hence, no energy will be found in the normal mode of the harmonic oscillator. Thus, within perhaps 20% or so for cases of interest, we obtain the estimate

$$\tilde{u}_x(t) = -\frac{4a_1 V_0\, \omega q \sin \omega t}{3\Delta_m\, m_i(\omega^2-\Omega_i^2)} \tag{A.6}$$

To find the distribution $f(\psi)$ of the angle of incidence, we must integrate the total velocity $u_x = \tilde{u}_x + \bar{u}_x$ to obtain the displacement x(t) and hence the time of impact, which we take to be the *first* time at which x = 0. Note that an ion can strike the surface only if its position x is closer to the surface than it has ever been previously. This is no restriction when $\rho_v/\Delta_m \ll \theta$, since in this case $\tilde{u}_x \ll \bar{u}_x$, and ions will always strike the surface at an angle $\psi \approx \theta$. When $\rho_v/\Delta_m > \theta$, however, the ions will not approach the surface monotonically, but will oscillate at a greater velocity than the velocity at which they drift towards the wall. The corresponding oscillations in x(t) have local minima x_{min} which gradually approach the surface at x = 0. It is important to note that, on impact, an ion must have been within a distance $(2\pi/\omega)\bar{u}_x = (2\pi/\omega)\bar{u}_\parallel \sin\theta$ of a local minimum $x_{min} < 0$, otherwise it would have come closer to the surface on a previous oscillation.

Using Eq. (16) for $\bar{u}_x$ and Eq. (A.6) for $\tilde{u}_x$ and integrating over time gives the orbit of an ion

$$x(t) \approx -\bar{u}_\parallel\, t \sin\theta + \frac{4V_0\, qa_1 \cos\omega t}{3\Delta_m\, m_i(\omega^2-\Omega_i^2)} + x_i \tag{A.7}$$

$$z(t) = \bar{u}_\parallel\, t \tag{A.8}$$

where x_i is an integration constant. In the $\rho_v/\Delta_m \ll \theta$ limit, the $\bar{u}_\parallel\, t \sin\theta$ term in Eq. (A.7) is dominant, and the angle $\psi = -dx/dz$ is clearly equal to θ. In the opposite limit, $\rho_v/\Delta_m > \theta$, of interest here, the $\bar{u}_\parallel\, t \sin\theta$ term may be neglected in Eq. (A.7). Then, expanding the cos function about -1, estimating $\bar{u}_\parallel = (2qV_0/m_i)^{1/2}$ and eliminating t from Eqs (A.7) and (A.8), the orbit x(z) near x_{min} is

$$x \approx x_{min} + \frac{z^2 a_1}{3\Delta_m\,(1-\Omega_i^2/\omega^2)} \tag{A.9}$$

where we identify

$$x_{min} = x_i - \frac{4V_0\, qa_1}{3\Delta_m\,(\omega^2-\Omega_i^2)} \tag{A.10}$$

The angle of incidence $\psi = -dx/dz$ in this limit, evaluated at impact (x = 0), is therefore

$$\psi \approx \tan\psi = \left(\frac{-4a_1\, x_{min}}{3\Delta_m\,(1-\Omega_i^2/\omega^2)}\right)^{1/2} \tag{A.11}$$

The maximum possible ψ occurs when $x_{min} = -(2\pi/\omega)\bar{u}_\parallel \sin\theta$ and is

$$\psi_m \approx 2^{7/4}\left(\frac{\pi a_1}{3}\right)^{1/2}\left(\frac{\theta\rho_v}{\Delta_m}\right)^{1/2}\left(\frac{\omega}{\Omega_i}-\frac{\Omega_i}{\omega}\right)^{-1/2} \tag{A.12}$$

Since, on impact, x_{min} is equally likely to be between 0 and $-(2\pi/\omega)\bar{u}_\parallel \sin\theta$, the distribution over ψ will be proportional to $(d\psi/dx_{min})^{-1}$ which, according to Eq. (A.11), is proportional to ψ. Hence the normalized distribution $f(\psi)$ is

$$f(\psi) = \frac{\psi}{2\psi_m^2} \qquad \text{for } \psi \le \psi_m$$
$$= 0 \qquad \text{for } \psi > \psi_m \tag{A.13}$$

The results derived in this Appendix are valid for $\rho_v/\Delta_m < \theta^{1/2}$, the limit of validity of Eq. (16). The expression for $f(\psi)$ also requires $\rho_v/\Delta_m > \theta$. At lower densities, where $\rho_v/\Delta_m < \theta$ applies, the distribution $f(\psi)$ approaches the delta function, $\delta(\psi-\theta)$. At higher densities, for which $\rho_v/\Delta_m > \theta^{1/2}$ holds, a numerical calculation of the ion orbits is necessary, but the trend will be towards larger ψ, approaching 90° when Eq. (6) is satisfied, i.e. when the ions are fully unmagnetized in the sheath. As an example, choosing parameters such that $\psi_m = 2(\theta\rho_v/\Delta_m)^{1/2}$, we obtain for $\theta = 5°$ that the limits of validity of Eq. (A.12) are $9° < \psi_m < 17°$. This is range over which the sputtering is typically very sensitive to ψ. Moreover, for most energies and ion species of interest, the sputtering rate is fairly insensitive to ψ in the range between 20°

and 90°, varying by no more than a factor of two, and so the sputtering rate can be estimated roughly, even without performing detailed calculations of the ion orbits in the $\rho_v/\Delta_m > \theta^{1/2}$ regime.

ACKNOWLEDGEMENTS

The authors wish to thank F.W. Perkins for stimulating conversations on sheath physics, and M. Bureš for many discussions of impurity data in tokamak plasmas. Useful conversations with S.N. Golovato, J. Jacquinot, W.S. Lawson, G.M. McCracken, M. Stamp and J.A. Tagle are also gratefully acknowledged.

This work was supported by the United States Department of Energy, under grant No. DE-FG02-88ER53263 and under contract No. DE-AC02-78ET51013.

REFERENCES

[1] BUREŠ, M., JACQUINOT, J., KAYE, A., BRINKSCHULTE, H., LAWSON, K.D., TAGLE, J.A., Plasma Phys. **30** (1988) 149.

[2] MANNING, H.L., TERRY, J.L., LIPSCHULTZ, B., et al., Nucl. Fusion **26** (1986) 1665.

[3] LEHRMAN, I.S., COLESTOCK, P.L., GREENE, G.J., et al., in Applications of Radiofrequency Power to Plasmas (Proc. 7th Top. Conf. Kissimmee, FL, 1987), American Institute of Physics, New York (1987) 274.

[4] STRATTON, B.C., MOOS, H.W., HODGE, W.L., et al., Nucl. Fusion **24** (1984) 767.

[5] BEHRISCH, R., WESNER, F., WIELUNSKI, M., NOTERDAEME, J.-M., TAGLAUER, E., in Controlled Fusion and Plasma Physics (Proc. 14th Eur. Conf. Madrid, 1987), Vol. 11D, Part II, European Physical Society (1987) 778.

[6] EQUIPE TFR, Plasma Phys. **24** (1982) 615.

[7] TAMAI, H., ODAJIMA, K., MATSUMOTO, H., et al., Nucl. Fusion **26** (1986) 365.

[8] TAYLOR, R.J., JAMES, B.W., JIN, S.X., et al., in Plasma Physics and Controlled Nuclear Fusion Research 1982 (Proc. 9th Int. Conf. Baltimore, 1982), Vol. 3, IAEA, Vienna (1983) 251.

[9] D'IPPOLITO, D.A., MYRA, J.R., BUREŠ, M., STAMP, M., JACQUINOT, J., "Impurity release from Faraday screens", presented at IAEA Tech. Comm. Meeting on ICRH/Edge Physics, 2-5 Oct. 1989, Garching (Proceedings to appear in Fusion Engineering and Design), in press.

[10] PURI, S., Phys. Rev. Lett. **61** (1988) 959.

[11] ITOH, K., FUKUYAMA, A., ITOH, S.-I., Comments Plasma Phys. Controll. Fusion **10** (1986) 91.

[12] PERKINS, F.W., Nucl. Fusion **29** (1989) 583.

[13] LANGLEY, R.A., BOHDANSKY, J., ECKSTEIN, W., et al., in Data Compendium for Plasma-Surface Interactions, Nucl. Fusion Special Issue (1984) 61, and Corrigenda in Nucl. Fusion **24** (1984) 1683; Sputtering by particle Bombardment I (BEHRISCH, R., Ed.), Springer-Verlag, New York (1981); ECKSTEIN, W., BIERSACK, J.P., Z. Phys., B. **63** (1986) 109.

[14] CHAN, C.C., JIN, Z.-J., WHITAKER, C., J. Appl. Phys. **62** (1987) 1633.

[15] CHO, M.H., HERSHKOWITZ, N., INTRATOR, T., J. Vac. Sci. Technol., A **6** (1988) 2978.

[16] BLETZINGER, P., FLEMMING, M.J., J. Appl. Phys. **62** (1987) 4688.

[17] KELLER, J.H., PENNEBAKER, W.B., IBM J. Res. Develop. **23** (1979) 3.

[18] GODYAK, V.A., in Soviet Radio Frequency Research, Delphic Associates, Falls Church, VA (1986); and references therein.

[19] LIEBERMAN, M.A., IEEE Trans. Plasma Sci. **PS-16** (1988) 638.

[20] GRAVES, D.B., J. Appl. Phys. **62** (1987) 88.

[21] JACQUINOT, J., and JET Team, Plasma Phys. Controll. Fusion **30** (1988) 1467; BUREŠ, M., BHATNAGAR, V., CORTI, S., et al., in Controlled Fusion and Plasma Heating (Proc. 15th Eur. Conf. Dubrovnik, 1988), Vol. 12B, Part II, European Physical Society (1988) 713.

[22] MYRA, J.R., D'IPPOLITO, D.A., GERVER, M.J., Faraday Screen Sheaths and Impurity Production during Ion Cyclotron Heating, Rep. LRC-89-5, Lodestar Research Corporation, Boulder, CO (1989).

[23] GOEDDE, C.G., LICHTENBERG, A.J., LIEBERMAN, M.A., Self-consistent Stochastic Electron Heating in Radio Frequency Discharges, Rep. UCB/ERL M88/29, Univ. California, Berkeley (1988).

[24] CHODURA, R., Phys. Fluids **25** (1982) 1628; DAYBELGE, U., BEIN, B., Phys. Fluids **24** (1981) 1190.

[25] ASCHER, U., CHRISTIANSEN, J., RUSSELL, R.D., Math. Comput. **33** (1979) 659.

[26] RUZIC, D.N., Bull. Am. Phys. Soc. **33** (1988) 2106 (paper 8W27).

[27] BEHRINGER, K., BOILEAU, A., BOMBARDA, F., et al., in Plasma Physics and Controlled Nuclear Fusion Research 1986 (Proc. 11th Int. Conf. Kyoto, 1986), Vol. 1, IAEA, Vienna (1987) 197.

[28] McCRACKEN, G.M., STANGEBY, P.C., Plasma Phys. Controll. Fusion **27** (1985) 1411.

[29] BUREŠ, M., JACQUINOT, J., STAMP, M., LAWSON, K., THOMAS, P., "ICRH/Plasma Edge Interaction in JET with Beryllium Gettering", presented at IAEA Tech. Comm. Meeting on ICRH/Edge Physics, 2-5 Oct. 1989, Garching (Proceedings to appear in Fusion Engineering and Design), in press.

[30] CATTO, P.J., MYRA, J.R., Phys. Fluids, B **1** (1989) 1193; CHIU, S.C., CHAN, V.S., Neoclassical Transport in the Presence of RF, Rep. GA-A19437, General Atomics, San Diego, CA (1988), and references therein.

[31] TFR Group and SAND, F., Nucl. Fusion **25** (1985) 1719.

(Manuscript received 4 April 1989
Final manuscript received 18 December 1989)